MYC inhibition induces metabolic changes leading to accumulation of lipid droplets in tumor cells

Hanna Zirath[a], Anna Frenzel[a], Ganna Oliynyk[a,b], Lova Segerström[c], Ulrica K. Westermark[a], Karin Larsson[a], Matilda Munksgaard Persson[d], Kjell Hultenby[e], Janne Lehtiö[f], Christer Einvik[g], Sven Påhlman[d], Per Kogner[c], Per-Johan Jakobsson[b], and Marie Arsenian Henriksson[a,1]

[a]Department of Microbiology, Tumor and Cell Biology, Karolinska Institutet, SE-171 77 Stockholm, Sweden; [b]Department of Medicine, Karolinska Institutet, SE-171 76 Stockholm, Sweden; [c]Childhood Cancer Research Unit, Astrid Lindgren's Children's Hospital, Department of Women's and Children's Health, Karolinska Institutet, SE-171 76 Stockholm, Sweden; [d]Center for Molecular Pathology, Department of Laboratory Medicine, Skåne University Hospital, Lund University, SE-205 02 Malmö, Sweden; [e]Department of Laboratory Medicine, Karolinska Institutet, SE-141 83 Stockholm, Sweden; [f]Department of Oncology-Pathology, Karolinska Institutet and Science for Life Laboratory, Clinical Proteomics Mass Spectrometry, SE-171 21 Solna, Sweden; and [g]Department of Pediatrics, University Hospital of North-Norway, N-9038 Tromsø, Norway

Edited* by George Klein, Karolinska Institutet, Stockholm, Sweden, and approved May 8, 2013 (received for review December 23, 2012)

The *MYC* genes are the most frequently activated oncogenes in human tumors and are hence attractive therapeutic targets. *MYCN* amplification leads to poor clinical outcome in childhood neuroblastoma, yet strategies to modulate the function of MYCN do not exist. Here we show that 10058-F4, a characterized c-MYC/Max inhibitor, also targets the MYCN/Max interaction, leading to cell cycle arrest, apoptosis, and neuronal differentiation in *MYCN*-amplified neuroblastoma cells and to increased survival of *MYCN* transgenic mice. We also report the discovery that inhibition of MYC is accompanied by accumulation of intracellular lipid droplets in tumor cells as a direct consequence of mitochondrial dysfunction. This study expands on the current knowledge of how MYC proteins control the metabolic reprogramming of cancer cells, especially highlighting lipid metabolism and the respiratory chain as important pathways involved in neuroblastoma pathogenesis. Together our data support direct MYC inhibition as a promising strategy for the treatment of MYC-driven tumors.

mitochondria | fatty acid oxidation | oxidative phosphorylation | small molecule | cancer therapy

The MYC proteins (here referring to c-MYC and MYCN) are helix–loop–helix leucine zipper transcriptional regulators that control a variety of normal cellular functions by forming specific DNA-binding heterodimers with the Max protein (1, 2). Deregulated MYC expression is a key event for malignant transformation by inducing multiple tumor-promoting events, including uncontrolled cell proliferation, cell mass expansion, and genomic instability, and contributes to the genesis of a large number of human cancers (1–3). Metabolic reprogramming is essential in cancer cells for adaptation to the tumor microenvironment and for maintenance of tumor growth (4, 5). MYC is a potent regulator of these processes by inducing increased glycolysis and glutaminolysis (6, 7) and by stimulating mitochondrial biogenesis and function (8–10). Several lines of experimental evidence support MYC as a therapeutic target (3, 6, 11, 12). Its down-regulation is sufficient to cause tumor regression, mediated by cell growth arrest, apoptosis, senescence, and/or differentiation in MYC-driven animal models (13), and systemic MYC inhibition in mice has been reported to cause minimal and reversible side effects for normal cells and tissues (14).

Neuroblastoma (NB) is a pediatric cancer of the sympathetic nervous system. In this malignancy, *MYCN* oncogene activation through amplification is an important hallmark of advanced tumor stage and poor prognosis, characterizing one subset of high-risk patients prone to resistant disease and progression despite intensive multimodal therapy (15). Importantly, down-regulation of MYCN expression results in apoptosis, decreased proliferation, and/or neuronal differentiation in NB cells in vitro (16, 17). Consequently, MYCN is an attractive target for therapy in high-risk NB.

Small molecules inhibiting protein–protein interactions represent a challenging yet desirable strategy for cancer therapy. The low-molecular-weight compound 10058-F4 has been shown to bind c-MYC in vitro, to disrupt c-MYC/Max interaction, and to inhibit the growth of c-MYC-transformed cells (11, 18) but failed to elicit efficacy in vivo (19). Here, we demonstrate 10058-F4 to target NB cells with high MYCN expression and to induce antitumorigenic responses in relevant experimental models of NB. We also show that inhibition of MYCN is accompanied by accumulation of intracellular lipid droplets in NB cells owing to mitochondrial dysfunction.

Results

10058-F4 Targets the MYCN/Max Interaction in NB Cells, Resulting in Growth Inhibition and Apoptosis. On the basis of sequence similarity between MYCN and c-MYC, we addressed whether 10058-F4 could interfere with MYCN/Max dimerization. Indeed, MYCN/Max interaction was inhibited in situ after treatment of *MYCN*-amplified (MNA) NB cells with 10058-F4 (Fig. 1 *A* and *B*). Neither the total levels of MYCN (Fig. 1*A*) nor Max was affected at the early time point analyzed. These results were corroborated in a second MNA cell line in which less MYCN protein was coimmunoprecipitated with Max after 10058-F4-treatment (Fig. 1*C*). As expected (18), less c-MYC was also retrieved in Max immunoprecipitations from c-MYC–expressing p493-6 B cells after incubation with 10058-F4 compared with control (Fig. 1*C*). Extended treatment of MNA NB cell lines revealed a concentration-dependent decrease in MYCN protein levels (Fig. 1*D*), which was blocked by proteasome inhibition (Fig. S1*A*), suggesting involvement of proteasome-mediated proteolysis in response to interference with the MYCN/Max interaction. We also observed decreased MYCN/Max and c-MYC/Max DNA binding after 10058-F4 treatment (Fig. 1*E*), probably reflecting reduced total levels of MYCN (Fig. 1*D*) and of c-MYC. Hence, 10058-F4 targets the MYCN/Max interaction, ultimately resulting in decreased MYCN levels in NB cells.

If 10058-F4 targets MYCN in addition to c-MYC, we would expect growth-suppressive effects in NB cells with high MYCN expression. Indeed, 10058-F4 induced both G1 arrest and apoptosis to a higher extent in MNA cell lines compared with non-MNA cells (Fig. 2 *A* and *B*), and Tet21N cells with high

Author contributions: H.Z., A.F., J.L., S.P., P.K., and M.A.H. designed research; H.Z., A.F., G.O., L.S., U.K.W., K.L., M.M.P., and K.H. performed research; C.E. contributed new reagents/analytic tools; H.Z., A.F., G.O., P.K., P.-J.J., and M.A.H. analyzed data; and H.Z., A.F., and M.A.H. wrote the paper.

The authors declare no conflict of interest.

*This Direct Submission article had a prearranged editor.

Freely available online through the PNAS Open Access option.

[1]To whom correspondence should be addressed. E-mail: marie.henriksson@ki.se.

This article contains supporting information online at www.pnas.org/lookup/suppl/doi:10.1073/pnas.1222404110/-/DCSupplemental.

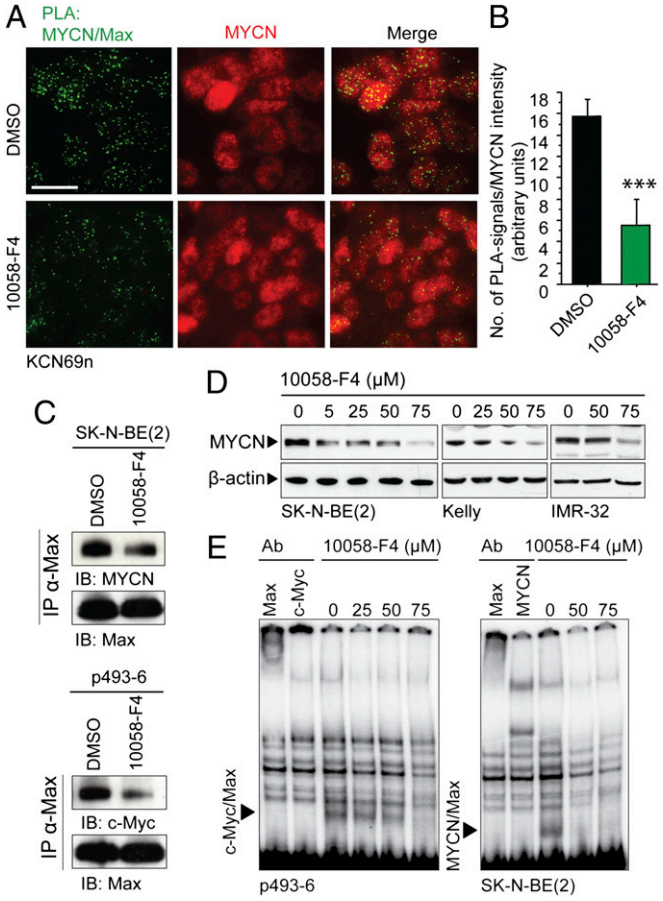

Fig. 1. 10058-F4 interferes with the MYCN/Max interaction. (*A*) Proximity ligation assay (PLA) on MYCN/Max interaction after 6 h treatment with 75 μM 10058-F4 in KCN69n cells (***$P < 0.0001$, mean ± SD, $n = 5$). (*Left*) Green signals indicate close proximity between MYCN and Max. (*Center*) Immunofluorescence of MYCN expression from the same cell sections. (*Right*) Merged PLA and MYCN signals. (Scale bar, 20 μm.) (*B*) Quantification of the PLA in *A*. (*C*) Coimmunoprecipitation (IP) of Max/c-MYC and Max/MYCN from cell extracts treated in vitro with 100 μM 10058-F4. (*D*) Western blot analysis of MYCN expression in MNA NB cell lines treated for 48 h with 10058-F4 at indicated concentrations. (*E*) EMSAs after treatment in culture with 10058-F4 for 48 h at indicated concentrations. Specific antibodies (Ab) were used to identify DNA-bound c-Myc/Max and MYCN/Max protein complexes, indicated with arrows to the left.

MYCN expression were more sensitive to 10058-F4–induced apoptosis compared with low MYCN-expressing cells (Fig. S1*B*). Furthermore, treatment of MNA NB cells with 10058-F4 decreased their capacity to grow in an anchorage-independent manner and inhibited cell migration (Fig. S1 *C* and *D*). These data suggest that 10058-F4 targets NB cells that depend on maintained MYC expression.

10058-F4 Induces NB Cell Differentiation and TrkA Expression. MYCN suppresses neuronal differentiation, whereas MYCN inhibition in vitro results in differentiation of MNA NB cells (16, 20). This led us to ask whether 10058-F4 has the capacity to induce differentiation in NB cells. Neurite outgrowth was evident after continuous incubation of two MNA cell lines with sublethal concentrations of 10058-F4 (Fig. 2*C* and Fig. S1*E*). The neurotrophin receptor TrkA is a reliable genetic marker of differentiation and a strong predictor of a favorable prognosis in NB, and high expression in tumors correlates inversely with MNA (16, 17, 21). Both *TRKA* mRNA and protein were up-regulated by 10058-F4 in the two differentiated MNA NB cell lines (Fig. 2*D* and Fig. S1*F*). Functional induction of the TrkA receptor by 10058-F4 was further supported because nerve growth factor, the high-affinity ligand of TrkA (16), potentiated the differentiated morphology of 10058-F4–treated cells by increasing both the number and length of neurite protrusions (Fig. 2*C*). Thus, 10058-F4 is sufficient to relieve MYCN-mediated suppression of NB cell differentiation.

10058-F4 Elicits Therapeutic Responses in NB Tumor Models. We next evaluated the therapeutic response in the preclinical TH-*MYCN* transgenic mouse model, which recapitulates human high-risk NB (22), and observed that treatment significantly prolonged the survival of tumor-bearing mice (Fig. 2*E*). We also examined the response in a s.c. MNA NB xenograft model using highly aggressive SK-N-BE(2) cells. Although the effect of 10058-F4 on overall tumor growth was not significant (Fig. S1*G*), there was a significant delay until the tumors increased two-, four-, or sixfold in volume (Fig. S1*H*). Furthermore, immunohistochemistry staining revealed 41% more cleaved caspase-3 in sections from treated compared with control tumors, demonstrating that 10058-F4 induced apoptosis in the NB xenografts (Fig. S1 *I* and *J*). Hence, in vivo effects can be achieved using a small molecule that targets the MYC/Max interaction.

MYC Inhibition Results in Lipid Accumulation in Tumor Cells. An intriguing observation after 10058-F4 treatment was that vesicle-like particles not present in untreated cells accumulated over time throughout the cell cytoplasm. Staining of 10058-F4–treated MNA NB cells with Oil Red O revealed that the vesicles contained fat (Fig. 3*A*). This finding was supported by transmission electron microscopy (Fig. 3*B*). To assess whether the increase in lipid droplets could be attributed to direct targeting of MYCN we transfected MNA NB cells with *MYCN*-shRNA. A marked induction of lipid accumulation was indeed observed after MYCN down-regulation (Fig. 3 *C* and *D*). Next we investigated the effect of the bromodomain inhibitor JQ1, recently shown to inhibit c-*MYC* transcription (23, 24). Strikingly, JQ1 decreased the MYCN levels, followed by formation of lipid droplets (Fig. 3 *E* and *F*), again showing that MYCN inhibition leads to lipid accumulation in MNA NB cells.

Additionally, we used isogenic rat embryonic fibroblast cell lines with different *c-myc* status to address whether this finding also applies to c-MYC down-regulation. Untreated HO15.19 *c-myc* null cells contained high amounts of stainable lipid droplets compared with the low levels present in parental TGR-1 and in *c-myc* overexpressing HOmyc3 cells (Fig. 3*G*). As expected, treatment with 10058-F4 did not impact on the already high lipid content in the HO15.19 cells. However, a robust increase in lipids was observed in the TGR-1 cells and to an even greater extent in the HOmyc3 cells after 10058-F4-incubation (Fig. 3*G*).

Lipids also accumulated in response to 10058-F4 treatment in additional tumor cell lines analyzed (Fig. S2*A*). In contrast, treatment of primary, nontransformed human lung and dermal fibroblasts did not result in accumulated lipids (Fig. S2*B*). Importantly, out of three cytotoxic drugs tested, only cisplatin treatment led to elevated levels of stainable lipids in NB cells at sublethal concentrations (Fig. S2*C*). Whereas cisplatin did not affect proliferation, both etoposide and camptothecin induced arrest in the G2 phase of the cell cycle (Fig. S2*D*), indicating that growth suppression per se does not lead to lipid accumulation. Finally, we observed that sections from 10058-F4–treated TH-*MYCN* tumors generally contained more fat droplets compared with those from vehicle-treated tumors (Fig. S2*E*). Together, these findings demonstrate that inhibition of MYCN or c-MYC can result in accumulation of lipids in cells with elevated MYC-regulated metabolism.

10058-F4 Is Highly Selective Against the MYC-Signaling Pathway in NB Cells. To expand our understanding of how 10058-F4 affects NB cells, we applied quantitative proteomics on MNA NB

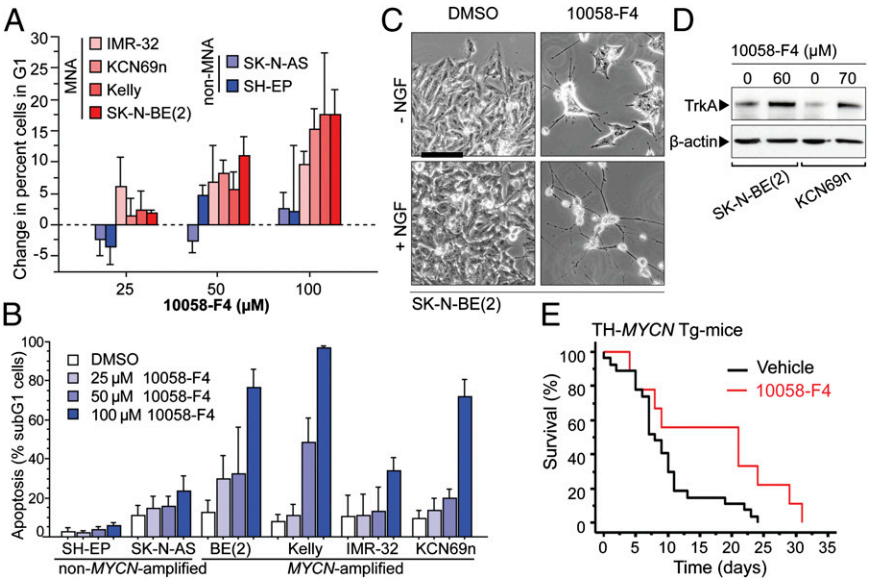

Fig. 2. 10058-F4 targets MNA NB cells and induces neuronal differentiation and therapeutic effects in vivo in MNA NB. (*A*) Change in the percentage of NB cells in the G1 phase of the cell cycle compared with untreated control after treatment with indicated concentrations of 10058-F4 for 24 h (mean ± SD, $n = 3$). (*B*) 10058-F4–induced cell death in MNA and non-MNA NB cell lines at indicated concentrations as assessed by the percentage of cells with subG1 DNA content (mean ± SD, $n = 3$, 72 h). BE(2) indicates SK-N-BE(2) cells. (*C*) Morphological differentiation of SK-N-BE(2) cells in response to 10058-F4 (60 μM), nerve growth factor (NGF, 50 ng/mL), or in combination for 15 d. (Scale bar, 50 μm.) (*D*) Western blot shows TrkA expression after 15 d treatment with 10058-F4. (*E*) Kaplan-Meyer survival of 10058-F4–treated TH-*MYCN* mice. Two animals per treatment group were homozygous for the *MYCN* transgene, and the rest were heterozygous. The median number of days in treatment was 11 ($n = 27$) for control and 21 ($n = 9$) for 10058-F4–treated animals ($P = 0.0303$).

cells treated with 10058-F4. For comparison, we used the same cell line stably transduced with an inducible *MYCN*-shRNA to down-regulate MYCN. The levels of the majority of affected proteins were decreased both in response to 10058-F4 as well as to *MYCN*-shRNA (Table S1 and Datasets S1 and S2). Gene ontology (GO) predictions revealed a striking similarity in affected biological processes in response to both treatments (Fig. 4*A*). Notably there was a robust impact of 10058-F4 on downstream MYC-targets. Ingenuity analysis of regulated canonical cell signaling pathways demonstrated that the same processes were consistently impaired in both conditions, with the greatest effect seen on cellular activities associated with MYC, including protein translation and mitochondrial functions (Fig. 4*B* and Datasets S1 and S2). Importantly, Ingenuity analysis predicted MYCN and c-MYC to be the two most significantly affected transcription factors in response to both 10058-F4 as well as *MYCN*-shRNA (Fig. S3*A*). The proteomic data were validated using immunoblotting (Fig. S3*B*). Collectively, these data show that 10058-F4 targets MYC signaling in NB cells.

MYCN Inhibition Causes Respiratory Chain Impairment. To further dissect how 10058-F4 influences NB cell metabolism and consequently causes lipid accumulation, we compiled all proteins involved in respiration as well as carbohydrate, lipid, and amino acid metabolism found down-regulated in the two experimental settings (Tables S2 and S3). The majority of down-regulated metabolic proteins were those comprising the respiratory chain both in response to 10058-F4 and anti-*MYCN* shRNA (Fig. 5*A* and Tables S2 and S3), suggesting that these changes caused the observed lipid accumulation. Interestingly, the levels of many enzymes involved in catalyzing β-oxidation of fatty acids as well as essential factors regulating the citric acid cycle and glycolysis were also reduced after 10058-F4 treatment. In addition, several enzymes involved in amino acid metabolism were affected (Fig. 5 *A* and *B* and Table S2). Approximately half of the metabolism-related proteins down-regulated by 10058-F4 are reported MYC-target genes (Table S2).

Inhibition of Mitochondrial Respiratory Complexes and β-Oxidation Induce Lipid Accumulation. Interference with fatty acid β-oxidation during continued cellular fatty acid import or synthesis can lead to accumulation of lipids in nonadipose cells (25–27), and our proteomic data demonstrated that 10058-F4 decreased the expression of essential enzymes regulating fatty acid oxidation (Fig. 5 *A* and *B* and Table S2). Together with the observed effect on the respiratory chain (Fig. S3*C*), this suggests that alterations in the integrity of the respiratory chain in response to MYCN inhibition result in reduced capacity for oxidation of fatty acids in mitochondria. Increased lipid levels could indeed be observed in MNA NB cells after treatment with inhibitors of the respiratory chain as well as of β-oxidation, whereas two inhibitors of glycolysis did not affect the amount of lipid droplets (Fig. 5*C*). Conceivably, lipid accumulation in response to MYCN inhibition could also result from an imbalance in the decay time of MYC-mediated processes, causing lipid synthesis to exceed growth demands. Hence, to investigate the possibility that continued fatty acid biosynthesis may contribute to the accumulation of lipids, we treated NB cells with 10058-F4 in combination with inhibitors of fatty acid synthesis. Treatment with the fatty acid synthase (FASN) inhibitor cerulenin (28) at sublethal concentrations did not impact on the lipid accumulation induced by 10058-F4 (Fig. 5*D* and Fig. S2*F*). In contrast, 5-(Tetradecyloxy)-2-furoic acid (TOFA), which inhibits acetyl CoA carboxylase (ACC) (29), although it may also stimulate β-oxidation because of decreased levels of malonyl-CoA (29–31), almost completely blocked the 10058-F4–induced fat droplet formation (Fig. 5*D* and Fig. S2*F*). We also addressed the possibility that previously synthesized lipids, which would have been used in various cellular processes during continued proliferation, may accumulate after growth suppression in response to MYC inhibition. Hence, we pretreated cells with cerulenin to inhibit lipid synthesis before the addition of 10058-F4. Nevertheless, pretreatment did not influence the 10058-F4–induced lipid accumulation (Fig. S2*G*). Together these results support reduced oxidation, rather than continued synthesis of fatty acids or accumulation of previously synthesized lipids, as the major cause of lipid droplet formation in response to 10058-F4 treatment.

Given the fact that lipid accumulation occurred in response to inhibition of mitochondrial processes, we next assessed the long-term effects of 10058-F4 on the morphology of mitochondria in NB cells. Visualization with MitoTracker demonstrated that the networks of elongated mitochondrial structures seen in untreated MNA NB cells became shorter, and occasional ring-formed structures appeared in response to 10058-F4 (Fig. S3*D*). Transmission electron microscopy revealed that mitochondria from treated cells appeared lighter and contained less elaborate cristae patterns, indicating loss of mitochondrial proteins (Fig. 5*E*). These results are consistent with the observations that chronic depletion of c-MYC reduces mitochondrial mass, results in smaller and cristae-deficient mitochondria, and alters the dynamics of mitochondria fission and fusion, leading to reduced oxidative phosphorylation capacity (9, 10).

Finally we addressed the impact of affected metabolic proteins on NB patient survival using a clinical microarray data set representing 251 children (32). Gene expression corresponding to 20 of the metabolic proteins found down-regulated by 10058-F4 were available in this data set. Of these, 14 (70%) were found to positively correlate with high MYC pathway activity (Fig. S4 *A* and *B* and Table S2) and were also significantly associated with reduced event-free (Table S2) and/or overall survival (Fig. S4 *A* and *C* and Table S2). Taken together, our results strengthen the proposed function of MYC as an essential regulator of mitochondrial integrity in tumor cells. They also demonstrate that impairment of the respiratory chain by MYCN inhibition ultimately interferes with the oxidation of fatty acids, hence causing lipids to accumulate.

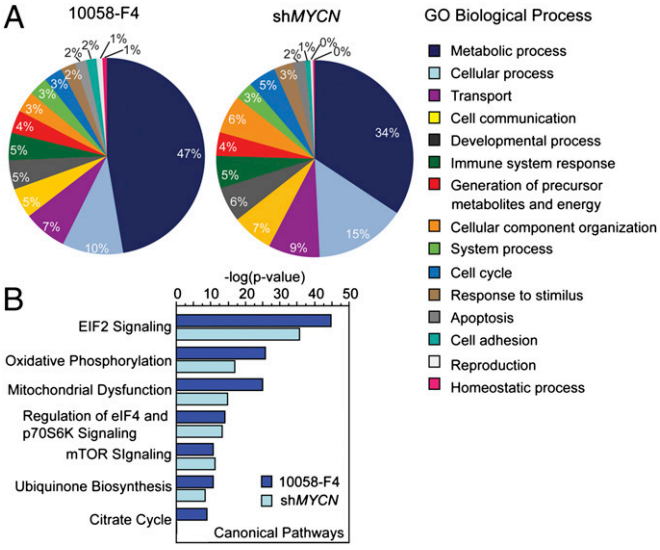

Fig. 4. Downstream MYC signaling pathways are targeted by 10058-F4. (*A*–*C*) Quantitative LC-MS/MS–based proteomic analysis using SK-N-BE(2) cells treated for 20 h with 10058-F4 (60 μM), or after 24 h induction of retrovirally transduced SK-N-BE(2) cells with anti-*MYCN* shRNA. Ingenuity software and PANTHER classification were used for data analysis and predictions. (*A*) GO analysis shows significantly affected biological processes. (*B*) The most significantly affected canonical cell signaling pathways in the two different conditions as indicated.

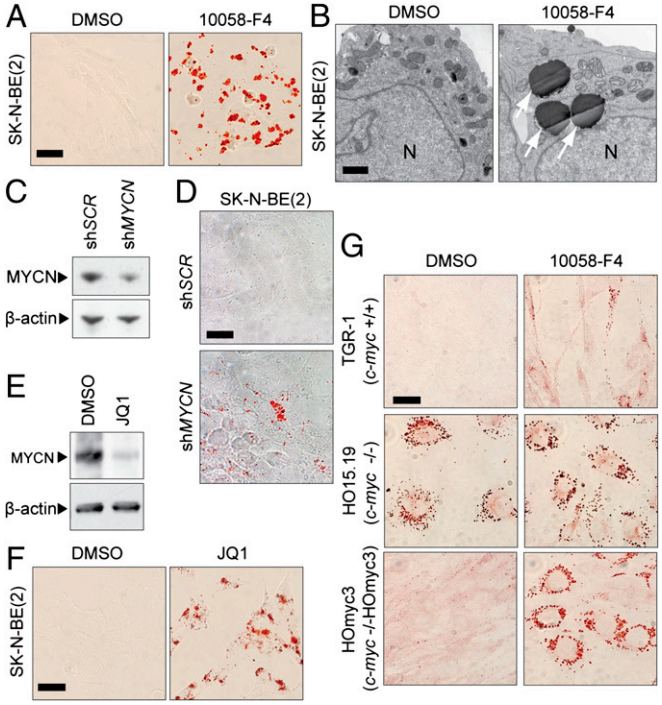

Fig. 3. MYC inhibition results in lipid accumulation. (*A*) Oil Red O staining of SK-N-BE(2) cells treated with 10058-F4 (60 μM) for 3 d. (*B*) Transmission electron microscopic pictures of SK-N-BE(2) cells treated with 10058-F4 (60 μM) for 8 d. Arrows indicate lipid droplets (N = nucleus). (Scale bar, 1 μm.) (*C* and *D*) Immunoblot of MYCN (*C*) and Oil Red O staining (*D*) 4 d after transfection of SK-N-BE(2) cells with scrambled (sh*SCR*) or anti-*MYCN* (sh*MYCN*) shRNA. (*E* and *F*) Immunoblot of MYCN (*E*) and Oil Red O staining (*F*) in response to JQ1 (2.5 μM) after 48 h and 3 d, respectively. (*G*) Oil Red O staining of rat embryonic fibroblasts with different *c-myc* status after treatment with 10058-F4 (100 μM) for 7 d. (Scale bars, 20 μm in all panels unless specified otherwise.)

Discussion

Given the important role of deregulated MYC in conferring tumor aggressiveness, its therapeutic targeting represents a compelling approach in cancer research (3, 11). Several groups have identified compounds that interfere with the interaction between c-MYC and Max (11). However, clinical development of these compounds, including 10058-F4, is limited by their relatively low potency. To date no reports exist on the activity of any compound on the binding between MYCN and Max, nor has it been shown that in vivo efficacy can be achieved by any small molecule interfering with MYC/Max. Here we demonstrate that 10058-F4 targets the interaction between MYCN and Max and that treatment is sufficient to delay tumor growth in vivo in two NB models. Using a proteomic approach we revealed a robust down-regulation of proteins involved in MYC-regulated biological processes, and MYCN and c-MYC were predicted as the top two most inhibited transcription factors, showing the MYC specificity of this small molecule. Collectively our data clearly demonstrate that 10058-F4 inhibits MYCN signaling in NB cells, resulting in cell cycle arrest, apoptosis, and/or differentiation, as well as reduction of tumor growth in aggressive mouse models of NB.

By serendipity we found that lipid accumulation occurs in response to 10058-F4 treatment. Importantly, the use of several alternative strategies to modulate the function of MYC, including isogenic cell lines, the MYC-inhibitory small molecule JQ1, and *MYCN*-RNA interference, demonstrated this effect to be MYC specific. Our data furthermore indicated that 10058-F4 elicited a lipid response in NB tumors in vivo. In contrast, inhibition of physiological MYC levels seems insufficient to induce accumulation of lipids because 10058-F4 treatment of primary non-transformed fibroblasts did not lead to increased lipid levels.

Lipid metabolism is an emerging field in cancer research, and increased de novo lipid synthesis driven by misexpression of lipogenic enzymes such as FASN and ATP Citrate Lyase (ACLY), as well as enhanced fatty acid β-oxidation, have been implicated in different cancers (28, 29, 33, 34). A possible link between MYC activity and lipid metabolism has not been thoroughly studied, and the few existing reports are contradictory,

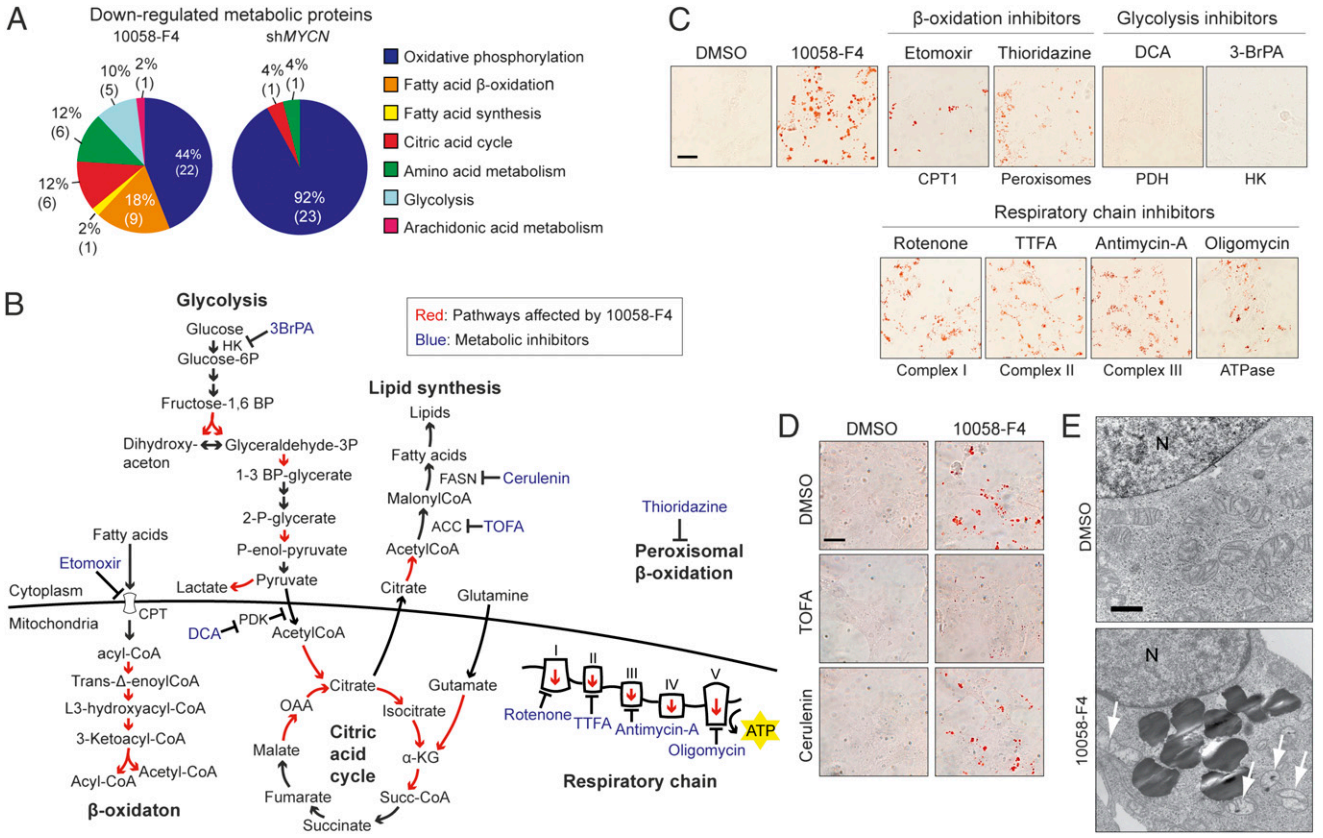

Fig. 5. Lipid accumulation occurs after inhibition of oxidative phosphorylation or β-oxidation and mitochondrial structure is perturbed by 10058-F4. (*A*) Number of down-regulated metabolism-related proteins of indicated categories, according to quantitative LC-MS/MS proteomic data (cutoff ratio: 0.667) from the two experimental conditions. (*B*) Schematic figure shows catalytic steps in metabolic pathways affected by 10058-F4, according to LC-MS/MS proteomic analysis data. Red arrow lines indicate down-regulation of enzymes involved in regulating the respective metabolic steps. (*C*) Oil Red O staining of lipid accumulation in SK-N-BE(2) cells in response to 3 d treatment with inhibitors of metabolic pathways as indicated. (Scale bar, 20 μm.) (*D*) Oil red O staining of SK-N-BE(2) cells treated with 10058-F4 in combination with TOFA or cerulenin for 3 d. (Scale bar, 20 μM). (*E*) Electron microscopic pictures of SK-N-BE(2) cells treated with 10058-F4 (50 μM) for 8 d. Arrows indicate affected mitochondria in the 10058-F4-treated cells. N = nucleus. (Scale bar, 1 μm.)

indicating that MYC can promote either fatty acid synthesis or fatty acid oxidation under different conditions (35, 36). Importantly, the metabolic reprogramming mediated by MYC during tumorigenesis was shown to depend on tissue type (37).

Accumulation of cytoplasmic lipids was recently demonstrated to occur in cancer cells after knockdown of carnitine palmitoyltransferase 1C (CPT1c), the brain-specific isoform of the β-oxidation rate-limiting enzyme (27). Interestingly, high CPT1c expression has been reported in NB cells (38), suggesting that enhanced β-oxidation activity may be an important metabolic feature in this disease. Our data demonstrated that inhibition of CPT1 and of peroxisomal β-oxidation indeed led to lipid accumulation in NB cells. Furthermore, treatment with 10058-F4 resulted in reduced expression of several enzymes directly involved in regulating oxidation of fatty acids. Notably, high expression of some of these enzymes was found to correlate with high MYC pathway activity and to poor survival in NB patients. In addition, cisplatin, which caused increased levels of lipid droplets in NB cells, is to our knowledge the only cytotoxic drug of the three tested that has been shown to interfere with fatty acid oxidation (39).

The finding that inhibition of ACC using TOFA prevented 10058-F4–induced lipid accumulation suggests that continued lipogenesis may also play a role in causing unoxidized lipids to accumulate after MYCN inhibition. However, TOFA treatment results in decreased malonyl-CoA levels (30) and hence inhibits lipid synthesis, although it may simultaneously stimulate β-oxidation (29, 31). Together with the observation that lipid droplet formation by 10058-F4 occurred although FASN was inhibited using cerulenin, this suggests that continued lipid synthesis or accumulation of previously synthesized lipids, in the setting of a reduced proliferation rate, were not major causes of the observed lipid droplet formation. This conclusion was further supported by the finding that simply halting proliferation using sublethal concentrations of etoposide or camptothecin did not cause accumulation of lipids. Collectively, our data imply that inhibition of β-oxidation leads to lipid accumulation after MYCN inhibition and suggest that aggressive NB tumors use fatty acids as an energy source.

The view that tumor cells primarily adapt metabolically by means of the Warburg effect has been challenged by reports showing a link between enhanced oxidative phosphorylation and tumorigenesis (40, 41). Likely, both aerobic glycolysis and efficient mitochondrial metabolism are important to support the energetic and biosynthetic demands of cancer cells (42). Several groups have established MYC's role in supporting mitochondrial biogenesis (9, 10, 35, 43), and the most obvious metabolic consequence observed in our proteomic analysis was the down-regulation of multiple subunits comprising all complexes of the respiratory chain. Importantly, inhibitors of different complexes of the respiratory chain all induced a robust lipid accumulation. Our data hence strengthen the emerging evidence for a defined role of MYC in stimulating oxidative phosphorylation, which may contribute to fulfill the bio-energetic demands of cancer cells by coordinating mitochondrial energy metabolism with cell proliferation and survival (8, 44).

Together our findings establish proof of concept for the development toward direct MYC-inhibition as a future approach to

inhibit tumor progression. Notably, these data further highlight the importance of alterations in lipid metabolism and the respiratory chain for MYCN-driven oncogenesis and demonstrate lipid accumulation to be a previously unknown consequence of inhibiting MYC. Our work also raises the question about possible implications of MYC in other human disorders, such as those contributing to the metabolic syndrome.

Materials and Methods

Detailed materials and methods are provided in *SI Materials and Methods*.

MYC/Max Interaction and DNA Binding. EMSA was performed as previously described (45), using protein lysates from cells treated with 10058-F4. For in vitro analysis of protein interaction between MYC/Max, extracts prepared from SK-N-BE(2) and p493-6 were incubated with 100 μM 10058-F4 or the corresponding volume of DMSO at 37 °C for 30 min before immunoprecipitation of Max. Proximity ligation assay was performed using Duolink in situ PLA (Olink Bioscience).

Apoptosis and Cell Cycle Assay. Apoptosis and cell cycle analysis was done by propidium iodide staining followed by flow cytometric analysis.

Oil Red O Staining of Lipids. Cells grown on coverslips were fixed in 4% (wt/vol) paraformaldehyde before staining with Oil Red O solution in 60% (vol/vol) isopropanol. For staining of fat on frozen tumor sections (5–10 μm thick), 0.5% Oil Red O in propylene glycol was used according to Nova Ultra Special Stain Kits (IHC WORLD). For visualization, bright-field images were captured at 63× magnification using an Axiovert 40 CFL inverted fluorescence microscope (Zeiss) and Axiovision Rel. 4.8 software.

Animal Experiments. Mice received vehicle or 10058-F4 (25 mg/kg) i.p., daily. In TH-*MYCN* animals, treatment was initiated when mice had palpable tumors. Animals were followed until the tumor progression and/or general health warranted killing. For xenograft assays, SK-N-BE(2) cells (20×10^6) were injected s.c. into the flanks of nude mice. Tumor size was measured daily.

LC-MS/MS Proteomic Analysis. Cells were fractionated into microsomal, membrane-associated and soluble proteins. Digested protein fractions were analyzed by LC-MS/MS using iTRAQ-8plex quantification on LTQ-Orbitrap Velos MS. Pathway analysis was performed by Ingenuity Pathways and PANTHER.

ACKNOWLEDGMENTS. We are grateful to and thank Professor C. V. Dang (University of Pennsylvania, Philadelphia, PA), Dr. V. Gogvadze (Karolinska Institutet, Stockholm, Sweden), and members of our laboratories for constructive discussions; Professor M. Schwab (German Cancer Research Center, Heidelberg, Germany) for the Tet21N cells; Professor G. Bornkamm (National Research Center for Environment and Health, Munich, Germany) for P493-6 cells; Professor J. Bradner (Dana Farber Cancer Institute, Boston, MA) for providing the JQ1 compound; and Professor R. N. Eisenman (Fred Hutchinson Cancer Research Center, Seattle, WA) for the Ab 143 MYC antibody. H.Z. was supported by a Graduate Fellowship from the Karolinska Institutet and A.F. by a Postdoctoral Grant from the Swedish Childhood Foundation. M.A.H. is a recipient of a Senior Investigator Award from the Swedish Cancer Society. This work was supported by grants from the Swedish Childhood Cancer Foundation, the Swedish Cancer Society, the Swedish Research Council, the KI Cancer Network, the Hedlund Foundation, and Karolinska Institutet.

1. Eilers M, Eisenman RN (2008) Myc's broad reach. *Genes Dev* 22(20):2755–2766.
2. Meyer N, Penn LZ (2008) Reflecting on 25 years with MYC. *Nat Rev Cancer* 8(12):976–990.
3. Vita M, Henriksson M (2006) The Myc oncoprotein as a therapeutic target for human cancer. *Semin Cancer Biol* 16(4):318–330.
4. Cairns RA, Harris IS, Mak TW (2011) Regulation of cancer cell metabolism. *Nat Rev Cancer* 11(2):85–95.
5. Dang CV (2012) Links between metabolism and cancer. *Genes Dev* 26(9):877–890.
6. Dang CV (2012) MYC on the path to cancer. *Cell* 149(1):22–35.
7. DeBerardinis RJ, Lum JJ, Hatzivassiliou G, Thompson CB (2008) The biology of cancer: Metabolic reprogramming fuels cell growth and proliferation. *Cell Metab* 7(1):11–20.
8. Dang CV (2011) Therapeutic targeting of Myc-reprogrammed cancer cell metabolism. *Cold Spring Harb Symp Quant Biol* 76:369–374.
9. Graves JA, et al. (2012) Mitochondrial structure, function and dynamics are temporally controlled by c-Myc. *PLoS ONE* 7(5):e37699.
10. Li F, et al. (2005) Myc stimulates nuclearly encoded mitochondrial genes and mitochondrial biogenesis. *Mol Cell Biol* 25(14):6225–6234.
11. Prochownik EV, Vogt PK (2010) Therapeutic targeting of Myc. *Genes Cancer* 1(6):650–659.
12. Sodir NM, Evan GI (2011) Finding cancer's weakest link. *Oncotarget* 2(12):1307–1313.
13. Felsher DW (2010) MYC inactivation elicits oncogene addiction through both tumor cell-intrinsic and host-dependent mechanisms. *Genes Cancer* 1(6):597–604.
14. Soucek L, et al. (2008) Modelling Myc inhibition as a cancer therapy. *Nature* 455(7213):679–683.
15. Maris JM (2010) Recent advances in neuroblastoma. *N Engl J Med* 362(23):2202–2211.
16. Edsjö A, Holmquist L, Påhlman S (2007) Neuroblastoma as an experimental model for neuronal differentiation and hypoxia-induced tumor cell dedifferentiation. *Semin Cancer Biol* 17(3):248–256.
17. Westermark UK, Wilhelm M, Frenzel A, Henriksson MA (2011) The MYCN oncogene and differentiation in neuroblastoma. *Semin Cancer Biol* 21(4):256–266.
18. Yin XY, Giap C, Lazo JS, Prochownik EV (2003) Low molecular weight inhibitors of Myc-Max interaction and function. *Oncogene* 22(40):6151–6159.
19. Guo J, et al. (2009) Efficacy, pharmacokinetics, tisssue distribution, and metabolism of the Myc-Max disruptor, 10058-F4 [Z,E]-5-[4-ethylbenzylidine]-2-thioxothiazolidin-4-one, in mice. *Cancer Chemother Pharmacol* 63(4):615–625.
20. Knoepfler PS, Cheng PF, Eisenman RN (2002) N-myc is essential during neurogenesis for the rapid expansion of progenitor cell populations and the inhibition of neuronal differentiation. *Genes Dev* 16(20):2699–2712.
21. Brodeur GM (2003) Neuroblastoma: Biological insights into a clinical enigma. *Nat Rev Cancer* 3(3):203–216.
22. Weiss WA, Aldape K, Mohapatra G, Feuerstein BG, Bishop JM (1997) Targeted expression of MYCN causes neuroblastoma in transgenic mice. *EMBO J* 16(11):2985–2995.
23. Delmore JE, et al. (2011) BET bromodomain inhibition as a therapeutic strategy to target c-Myc. *Cell* 146(6):904–917.
24. Mertz JA, et al. (2011) Targeting MYC dependence in cancer by inhibiting BET bromodomains. *Proc Natl Acad Sci USA* 108(40):16669–16674.
25. Dobbins RL, et al. (2001) Prolonged inhibition of muscle carnitine palmitoyltransferase-1 promotes intramyocellular lipid accumulation and insulin resistance in rats. *Diabetes* 50(1):123–130.
26. Ibdah JA, et al. (2001) Lack of mitochondrial trifunctional protein in mice causes neonatal hypoglycemia and sudden death. *J Clin Invest* 107(11):1403–1409.
27. Zaugg K, et al. (2011) Carnitine palmitoyltransferase 1C promotes cell survival and tumor growth under conditions of metabolic stress. *Genes Dev* 25(10):1041–1051.
28. Lupu R, Menendez JA (2006) Pharmacological inhibitors of fatty acid synthase (FASN)—catalyzed endogenous fatty acid biogenesis: A new family of anti-cancer agents? *Curr Pharm Biotechnol* 7(6):483–493.
29. Santos CR, Schulze A (2012) Lipid metabolism in cancer. *FEBS J* 279(15):2610–2623.
30. Pizer ES, et al. (2000) Malonyl-coenzyme-A is a potential mediator of cytotoxicity induced by fatty-acid synthase inhibition in human breast cancer cells and xenografts. *Cancer Res* 60(2):213–218.
31. Choi CS, et al. (2007) Continuous fat oxidation in acetyl-CoA carboxylase 2 knockout mice increases total energy expenditure, reduces fat mass, and improves insulin sensitivity. *Proc Natl Acad Sci USA* 104(42):16480–16485.
32. Oberthuer A, et al. (2006) Customized oligonucleotide microarray gene expression-based classification of neuroblastoma patients outperforms current clinical risk stratification. *J Clin Oncol* 24(31):5070–5078.
33. Liu Y (2006) Fatty acid oxidation is a dominant bioenergetic pathway in prostate cancer. *Prostate Cancer Prostatic Dis* 9(3):230–234.
34. Nieman KM, et al. (2011) Adipocytes promote ovarian cancer metastasis and provide energy for rapid tumor growth. *Nat Med* 17(11):1498–1503.
35. Fan Y, Dickman KG, Zong WX (2010) Akt and c-Myc differentially activate cellular metabolic programs and prime cells to bioenergetic inhibition. *J Biol Chem* 285(10):7324–7333.
36. Morrish F, et al. (2010) Myc-dependent mitochondrial generation of acetyl-CoA contributes to fatty acid biosynthesis and histone acetylation during cell cycle entry. *J Biol Chem* 285(47):36267–36274.
37. Yuneva MO, et al. (2012) The metabolic profile of tumors depends on both the responsible genetic lesion and tissue type. *Cell Metab* 15(2):157–170.
38. Reilly PT, Mak TW (2012) Molecular pathways: Tumor cells Co-opt the brain-specific metabolism gene CPT1C to promote survival. *Clin Cancer Res* 18(21):5850–5855.
39. Li S, et al. (2009) Transgenic expression of proximal tubule peroxisome proliferator-activated receptor-alpha in mice confers protection during acute kidney injury. *Kidney Int* 76(10):1049–1062.
40. Funes JM, et al. (2007) Transformation of human mesenchymal stem cells increases their dependency on oxidative phosphorylation for energy production. *Proc Natl Acad Sci USA* 104(15):6223–6228.
41. Weinberg F, et al. (2010) Mitochondrial metabolism and ROS generation are essential for Kras-mediated tumorigenicity. *Proc Natl Acad Sci USA* 107(19):8788–8793.
42. Ward PS, Thompson CB (2012) Metabolic reprogramming: A cancer hallmark even warburg did not anticipate. *Cancer Cell* 21(3):297–308.
43. Kim J, Lee JH, Iyer VR (2008) Global identification of Myc target genes reveals its direct role in mitochondrial biogenesis and its E-box usage in vivo. *PLoS One* 3(3):e1798.
44. Morrish F, Neretti N, Sedivy JM, Hockenbery DM (2008) The oncogene c-Myc coordinates regulation of metabolic networks to enable rapid cell cycle entry. *Cell Cycle* 7(8):1054–1066.
45. Mo H, Henriksson M (2006) Identification of small molecules that induce apoptosis in a Myc-dependent manner and inhibit Myc-driven transformation. *Proc Natl Acad Sci USA* 103(16):6344–6349.